Hartl H., Beer G. : "Computational Modeling of Reinforced Concrete Structures", Freytag B., Stebernjak B. (Hsg.), Festschrift zum 60. Geburtstag von Lutz Sparowitz, TU-Graz, pp. 105-114 (2000)

COMPUTATIONAL MODELING OF REINFORCED CONCRETE STRUCTURES

Helmut Hartl
TU-Graz, Institute for Structural Concrete

Gernot Beer
TU-Graz, Institute for Structural Analysis

ABSTRACT: Some issues of implementation of non linear finite element modeling of reinforced concrete structures are presented. Firstly, the elasto-plastic and the elasto-visco-plastic return algorithms are compared. A method is introduced which allows to simulate the elasto-plastic solution within an iterative procedure where no derivative of the yield function is needed. Secondly, the update of stresses within the supplementary slip model is discussed. The steel stress is initially overestimated due to the perfect bond assumption in the global stiffness matrix. The supplementary slip model relaxes this steel stress, thus even within a monotonically increasing external load a reverse loading situation is obtained numerically within the iterations. Two stress update techniques will be discussed, where this overestimation of the steel stress never results in plastic strain at the end of the iteration. Finally, the number of sample points employed for the stress recovery is discussed. Due to high stress gradients within a concrete structure, it seems to be necessary to employ sample points close to the boundary of the elements. This is studied numerically on a beam for the specific situation of reinforced concrete.

1 VISION

About two decades ago, on a visit to the University of Applied Sciences in Vienna, the second author was shown some visionary ideas by Lutz Sparowitz on an integrated approach to the design of reinforced concrete structures. The vision was of a completely automatic method of calculation and design. Starting from the general idea, for example the plan of constructing a bridge as part of a highway, the concept involved the automatic generation and transfer of all data until construction (reinforcement) plans were automatically generated.
A powerful data base is necessary to achieve this vision i.e. one which maintains all the information related to the object and passes information from the initial design to the analysis model and finally to the construction drawings. A major issue is the simplification of the actual structure for numerical analysis.
One option of numerical analysis is based on continuum mechanics. If the FE-method is applied for a comprehensive assessment of reinforced orprestressed concrete structures, the program must be able to account for the nonlinearity of the concrete and for the presence of the rebars. In such a model we may define every single rebar in the input phase but this information should be provided in digital form from the data base so no “hand” input should be necessary. The merit of such a scheme is that the amount of idealization is reduced considerably and that the structure response can be computed more accurately.
With this contribution, to mark the 60th birthday of Lutz Sparowitz, we hope to make a small contribution towards the realization of his vision.

2 INTRODUCTION

When the stress state is beyond the yield surface an iterative procedure has to be employed in order to return the stress state to the yield surface (Owen [1]). Several methods are available therefore which

can be split into two families. The elasto-plastic and the elasto-visco-plastic approaches. For some general constitutive models the former might be difficult to implement since the needed derivative of the yield function can be involved and the computation may be expensive. The latter does not need the derivative of the yield function. The crux is to find the right time step length in order to avoid unnecessary computation time on the one hand and to find convergence on the other hand. Here, these two algorithms are compared. A procedure which computes the elasto-plastic solution employing the elasto-visco-plastic theory is shown in section 3.

The rebars are incorporated according to the embedded approach (Elwi [2]). Within this approach, rigid bond is assumed at the level of the global stiffness matrix. Hence, the steel stress is overestimated due to the perfect bond assumption in the global stiffness matrix. The supplementary slip model is able to account for bond slip situations between rebars (or tendons) and concrete. Interface elements (Beer [3]) are introduced upon the known displacement field of the parent elements at the material level of the reinforcing steel (Hartl [4,5]) and the steel stress will be relaxed. Due to this scheme, a monotonically increasing external load will result in a reverse loading situation for the steel within the iterations, as shown in section 4. Two stress update techniques (Crisfield [6], Nyssen [7]) will be discussed. In both methods the overestimation of the steel stress at the beginning of the iteration does not result in a plastic strain at the end of the iteration.

The effect of the employed integration scheme on the numerical results is discussed in Zienkiewicz [8]. Concrete structures have in general a very high stress gradient and stresses have the maximum value at the boundaries of the domain. Thus, it seems to be necessary to employ sample points for the stress recovery and the subsequent integration of residual stresses to residual forces close to the boundary of the domain. The effect of the number and location of the sample points dependent on the physical nonlinearity of reinforced concrete is discussed on a numerical example in section 5.

The work presented here is implemented into a *B*oundary *E*lement / *F*inite *E*lement program (*BEFE* [9]). It provides a useful pre- and post-processing environment. Some tools for manipulating the reinforcement were added and an interface to a CAD program is in preparation [10].

3 CONVERGENCE IN NONLINEAR SITUATIONS

A material may behave elastically as long as a limiting stress state described by the yield surface is not exceeded. The displacements ($\mathbf{u}$) are obtained in a FE-analysis from the equation: $\mathbf{K}^{-1} \cdot \mathbf{F} = \mathbf{u}$, where $\mathbf{K}$ is the stiffness matrix and $\mathbf{F}$ are the applied forces. Strains ($\boldsymbol{\varepsilon}$) can be calculated from displacements by compatibility: $\boldsymbol{\varepsilon} = \mathbf{B} \cdot \mathbf{u}$, where $\mathbf{B}$ is the strain displacement matrix. These strains are related to stresses by employing a constitutive law. As long as this relation is linear and the stiffness corresponds to $\mathbf{K}$, equilibrium will be gained by default. Beyond the elastic limit, an iterative procedure is needed in order to fulfill the constitutive relation and equilibrium.

3.1 Review of the Elasto-Plastic Return

The general form of this procedure is

$$\boldsymbol{\sigma} = \boldsymbol{\sigma}_{el} - \Delta\lambda \cdot \mathbf{D} \cdot \frac{\partial Q}{\partial \boldsymbol{\sigma}} \qquad (1)$$

where

- $\boldsymbol{\sigma}$ corrected stress on the yield surface
- $\boldsymbol{\sigma}_{el}$ elastically predicted stress by the stiffness matrix
- $\Delta\lambda$ plastic strain rate multiplier (scalar)
- $\mathbf{D}$ constitutive matrix
- Q plastic potential function

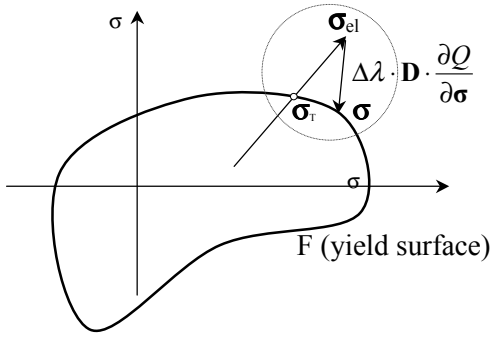

Figure 1 Return to the Yield Surface within the elasto-plastic approach

Eq. (1) must be evaluated at a distinct point within the applied increment. It can be computed at the transition point ($\boldsymbol{\sigma}_T$) of the elastically predicted increment with the yield surface (forward Euler procedure) or at the final point ($\boldsymbol{\sigma}$) where the stress is returned to the yield surface (backward Euler procedure). Evaluation of Eq. (1) at the end of the elastically predicted increment ($\boldsymbol{\sigma}_{el}$) is very

appealing, since this point is obtained straightforwardly. It can be viewed as a form of the backward Euler algorithm. A detailed discussion of these elasto-plastic algorithm for associative plasticity is presented in Crisfield [6].
The plastic strain rate multiplier $\Delta\lambda$ is a scalar which is obtained by two basic principles of elasto-plasticity. First, the plastic strain increment ($d\boldsymbol{\varepsilon}_p$) is perpendicular to the plastic potential function (Q); second, the stress state must never exceed the yield surface (F). The derivation for associative plasticity is given in Owen [1], for non associative plasticity $\Delta\lambda$ is given in Potts [11]

$$\Delta\lambda = \frac{F}{\frac{\partial F}{\partial \boldsymbol{\sigma}} \mathbf{D} \frac{\partial Q}{\partial \boldsymbol{\sigma}}} \qquad (2)$$

where F is the yield function

Eq (2) requires the derivative of the yield function and the derivative of the plastic potential function in order to obtain a stress state which is on (or more precisely: close to) the yield surface. If the increments are either not very small and/or the yield surface has a strong curvature, the computed stress state may have a considerably offset to the yield surface, no matter at which reference stress state $\Delta\lambda$ is computed. In general, the computed prediction of the corrected stress state lies outside the yield surface as shown in Figure 2.

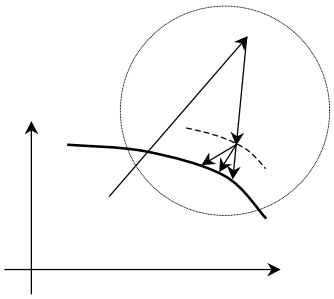

Figure 2 Offset of the numerical solution

In order to correct for this offset Crisfield [12] and Oritz [13] recommended to repeat the procedure (Eq. (1) and (2)) until the new stress state is sufficient close to the yield function ("operator splitting").

3.2 Review of the Elasto-Visco-Plastic Return

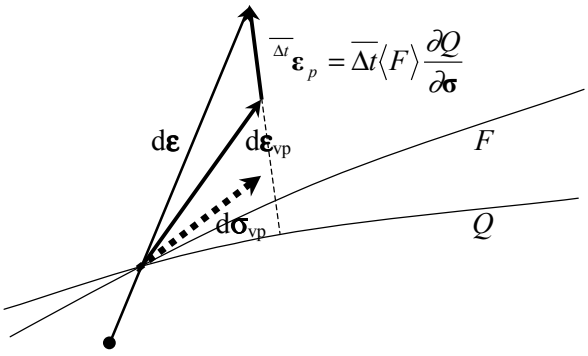

Figure 3 Illustration of the elasto-visco-plastic approach

A different procedure for the return to the yield surface is the elasto-visco-plastic approach. Perzyna proposed a theory [14,15] which is able to account simultaneously for two material behaviors: plasticity and rheology. It is assumed that plastic strains need time to develop. Hence, stress states beyond the yield surface ($F > 0$) are allowed for $t \neq \infty$ within this method. The viscosity parameter (η) is set to unity when rheology is not of interest. Then, the time (t) has no physical meaning any more, it will be reduced to a convergence parameter ($\bar{t}$) only. The stress at ($\bar{t} + \overline{\Delta t}$) within the return procedure to the yield surface is (Beer [16])

$$\overset{\bar{t}+\overline{\Delta t}}{\boldsymbol{\sigma}} = \overset{\bar{t}}{\boldsymbol{\sigma}} - \mathbf{D} \cdot \overline{\Delta t}\langle F\rangle \frac{\partial Q}{\partial \boldsymbol{\sigma}} \qquad (3)$$

where

$\overset{\bar{t}+\overline{\Delta t}}{\boldsymbol{\sigma}}$ stress at $\bar{t} + \overline{\Delta t}$

$\overline{\Delta t}\langle F\rangle \frac{\partial Q}{\partial \boldsymbol{\sigma}}$ visco-plastic strain increment within increment $\overline{\Delta t}$

step function:

$\langle F = 0$ if $F \leq 0$

$\langle F = f_{(F)}$ if $F > 0$

In the subsequent section only the product $\overline{\Delta t} \cdot \langle F$ is of interest any more. Thus, the value *1.0* is assigned to $\langle F$ if $F > 0$, this is $f_{(F)} = F^0$.

The strain rate $\partial Q / \partial \boldsymbol{\sigma}$ gets multiplied by the scalar $\overline{\Delta t} \cdot \langle F$. A small value of $\overline{\Delta t}$ should assure convergence but can be time consuming. On the other hand, a large time step can deteriorate the accuracy significantly. For some classical models, analytical time step lengths have been found by Cormeau [17], but not for the general case.

Zienkiewicz and Cormeau [18] have reported that a time step above a certain magnitude might result in an unstable iteration indicated by oscillation of residual forces. They gave an empirical rule for the time step and they limit this rule to associated plasticity with classical models. Applying this rule to general models with a non associative flow rule achieved indeed only limited success (Hartl [19]).

3.3 Proposed strain rate multiplier (time step)

Eq (1) and Eq (3) are similar. Both $\Delta\lambda$ and $\overline{\Delta t} \cdot \langle F$ can be referred to a scaling value for the strain rate. From the comparison of the two approaches follows that any $\Delta\lambda$ which produces a stress state along the path from the elastic prediction ($\boldsymbol{\sigma}_{el}$) to the return point on the yield surface ($\boldsymbol{\sigma}$) is acceptable within the iterative scheme. This multiplier, which results in the limiting stress state on the yield surface, is of interest for a fast computation.

$$F\left(\boldsymbol{\sigma} - \mathbf{D} \cdot \Delta\lambda \frac{\partial Q}{\partial \boldsymbol{\sigma}} \right) = 0 \qquad (4)$$

The condition given in Eq (4) can be fulfilled numerically by employing an iterative scheme. Here, the Newton root finding algorithm is employed. The derivative of F_n is approximated with the finite differences between two trial points.

$$\boldsymbol{\sigma}_{n+1} = \boldsymbol{\sigma}_n - \mathbf{D} \cdot \frac{F_n}{\dfrac{F_{n-1} - F_n}{\left\| \boldsymbol{\sigma}_{n-1} - \boldsymbol{\sigma}_n \right\|}} \cdot \frac{\partial Q}{\partial \boldsymbol{\sigma}_0} \qquad (5)$$

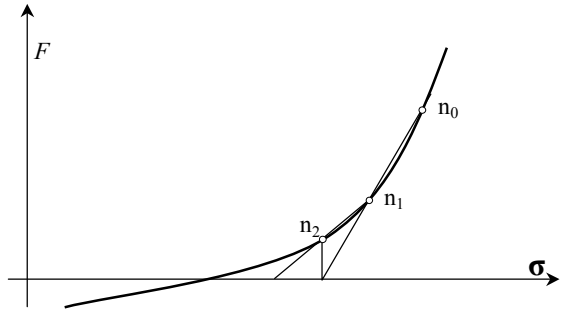

Figure 4 Iterative scheme for obtaining a stress state on the yield surface

The initial trial stress is $\boldsymbol{\sigma}_o = \boldsymbol{\sigma}_{el}$. Then, a small value is assigned to $\Delta\lambda$ and $\boldsymbol{\sigma}_1$ is computed by evaluation of Eq (1). For all subsequent steps Eq (5) applies and a fast convergence is obtained. The final stress is always on the yield surface.

There is no need within this method to compute the strain rate multiplier $\Delta\lambda$ or $\overline{\Delta t}$ explicitly, since the final stress state $\boldsymbol{\sigma}$, which is on the yield surface, is known at the end of the iteration process of Eq (5).

A merit of this approach is that the derivative of the yield function (F) is not needed in order to compute $\boldsymbol{\sigma}$. This is useful when the yield function is not smooth throughout the stress space, since only a smooth plastic potential function is necessary for the procedure presented here. This procedure is appealing as well when the derivative of the yield function is very involved and costly to compute.

An offset of the obtained stress state to the yield surface as indicated in Figure 2 cannot occur within the proposed method, the obtained stress state is always on the yield surface. Nevertheless, the direction of plastic flow (given by $\partial Q / \partial \boldsymbol{\sigma}$) changes usually its orientation within the iteration process to the final stress state on the yield surface ($\boldsymbol{\sigma}$). Hence, the solution can still be erroneous. Improvements can be made in different manners. One way is to split the elastic increment in sub increments as illustrated in Figure 5a. Another approach is to split the returning stress increment into sub increments as illustrated in Figure 5b.

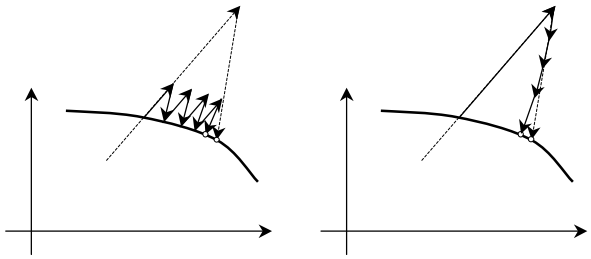

a) split of elastic increment b) split of exceeding increment

Figure 5 splitting of the stress increment

A third method is similar to this one illustrated in Figure 5b. The corrective increment is scaled by a fixed factor. Thus, only a certain ratio of the exceeding stresses are mapped as residual nodal forces and get reapplied on the domain. This follows the concept of visco-plasticity, where a stress state beyond the yield surface is allowed for $t \neq \infty$.

An automatic scaling procedure for the excess increments is proposed. The user defines the maximum ratio of the excess increment, which may be mapped as residual forces within one step. This ratio is called time scale. A value of *1.0* for the time scale gives the elasto-plastic solution. If the iterative procedure follows a convergent path, the residual forces will decrease with each iteration step. Divergence is indicated by increasing residual forces. For each divergent iteration the time scale is

reduced by 30%. When a convergent path is achieved again, the time scale will be increased by 10% for each stable iteration until the maximum time scale is reached again.

3.3.1 Application to Concrete

In this program (*BEFE*) concrete is modeled with Ottosen yield criterion [20]. The Ottosen criterion seems to have corners as shown in Figure 6b. However, a detailed investigation shows that it is smooth throughout the entire stress space. Even tough, within the classical elasto-plastic algorithm and employed normality rule for the flow, a small increment would be necessary at stress states in these regions where the yield surface has a strong curvature. In addition, the derivative of the yield function is very involved symbolically, and the numerical evaluation would be time consuming as well.
In order to account for mode I cracks in a simple but robust fashion the yield criterion is combined with Rankine tension cut off, which is not smooth. Additional edges are obtained at the intersection of the two surfaces. The edges could be rounded numerically if associated flow has to be considered. But the direction of plastic flow is not well known for concrete materials and neither of importance in many cases. Thus, the van Mises cylinder is employed as plastic potential surface.

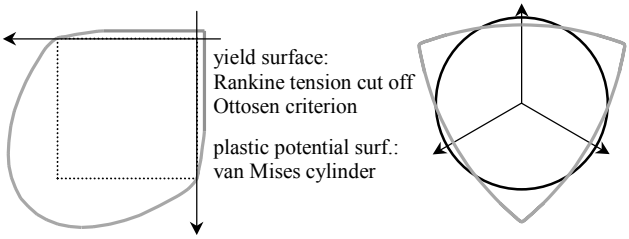

Figure 6 Constitutive model for concrete

4 SUPPLEMENTARY SLIP MODEL - STRESS UPDATE

When reinforcement is modeled utilizing the embedded approach (Elwi [2]) and Hartl [5]), the same displacement field is assigned to the parent element (2D/3D) and to the one dimensional rebar element. Perfect bond is obtained. A characteristic stress distribution along the rebar is shown in Figure 7b. Bond slip/tendon sliding can be accounted for at the material level by introducing interface elements supplementary between rebar and concrete after the displacement field has been computed (Hartl [4, 5]). Due to bond slip the steel stress can relax as indicated in Figure 7c.

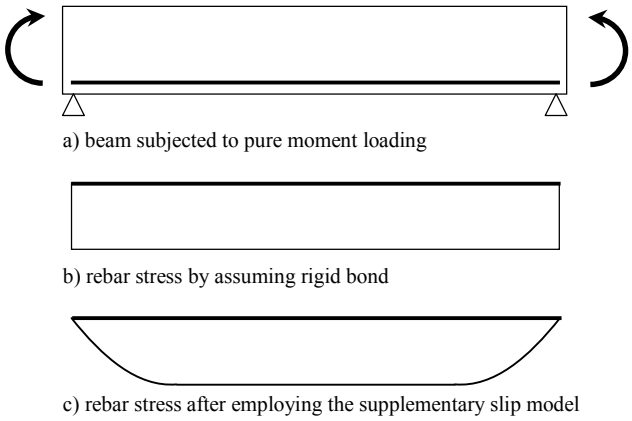

Figure 7 Stress distribution along the rebar

The basic idea of the supplementary slip algorithm is illustrated in Figure 8 on a truss analogy. The truss members are the rebars and the supports are the concrete. Since we account for slip, the supports are linked to the rebars by bond springs (which are implemented as continuous interface elements (Beer [3]). The strains of the parent element along the rebar path get integrated and are referred to prescribed displacements of the supports. These support displacements get transferred to the rebars by bond springs. The arising relative displacement of a rebar support node and the adjacent rebar node is referred to as bond slip. The differences of the forces in the rebar elements now, compared to forces in these elements with rigid bond, are forces due to bond slip. These forces are mapped back as residual nodal forces of the parent element. The interface forces need not to be considered within the residual forces. These forces act on both sides on the rebar and on the concrete but with opposite sign, thus these interface forces cancel out.

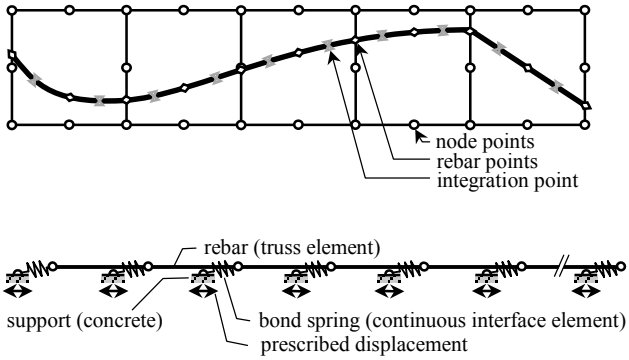

Figure 8 Illustration of the supplementary slip algorithm on a truss analogy

Within the standard loop over all parent elements, the strains of the rebars along the portion within the respective parent element are computed. After this loop is finished, the strains along each rebar are known and the supplementary slip algorithm may be invoked.

When stiffness terms for the interface elements are integrated, the stiffness modulus is obtained by relating the relative displacement between the rebar and the according concrete to the constitutive relation of the interface. The interface stiffness will decrease with increasing slip as indicated in Figure 9. Thus, an iterative scheme is needed.

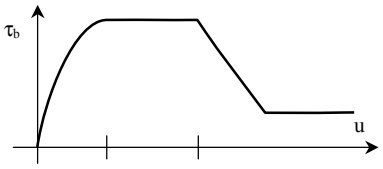

Figure 9 Generic form of the bond slip relation

Within this iterative scheme the slip will increase monotonically. The steel stress will be overestimated in the first iteration followed by a continuous unloading in all subsequent iterations. This causes no problems as long as the steel does not exceed the elastic limit as shown in Figure 10a. The numerical simulation of the load path might go from A over B in the first iteration to C and D in the subsequent iterations. However in nature the load path goes directly from A to D, since the slip arises simultaneously with the applied load.

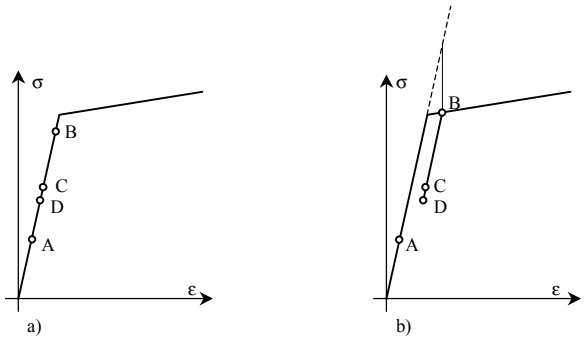

Figure 10 Loading path for the steel within the iterative process

Other, when the first prediction of the steel stress exceeds the elastic limit as shown in Figure 10b. A plastic strain increment applies to the steel. Further iterations unload the steel only elastically and result in an erroneous solution, since the plastic strain increment occurs only due to the iterative scheme, but it does not happen along loading from A to D. The strains get updated with the previous iteration as reference. This method is referred as “iterative strain update” in Chrisfield [6].

Updating the strains always from the beginning of the iterative scheme (point A) overcomes this lack. This is referred as “incremental strain update” in Chrisfield [6].

A remedy within the “iterative strain update” was proposed by Nyssen [7]. There, a plastic unloading back to the last converged reference state (point A) is allowed.

From an engineering point of view slip occurs preferable only at the beginning and at the end of the rebars. This is in regions where the utilization of the rebar is low and the rebar is far below the yield limit. Thus, situations according to Figure 10a are more likely to happen. When unbonded tendons are considered, slip occurs along the entire tendon between the two fixed ends. Stresses in these tendons are more or less constant along the entire tendon and nearly independent of the applied external load on the domain. A local concentration of strains in the concrete due to loading causes slip only instead of a localization of high tendon forces. Thus, yielding is not a criterion for unbonded tendons and situations shown in Figure 10b do not apply as long as the increments are not too big.

However, if the yield limit is exceeded in an unlucky situation and an “iterative strain update” is implemented more deformations will be obtained. In most cases more deformations are considered as an error on the save side.

The performance of the supplementary slip model will be investigated in this regard by several case studies and the scheme that seems to be most appropriate will be employed.

5 STRESS RECOVERY AND INTEGRATION OF RESIDUAL STRESSES

Concrete is only able to sustain a very small amount of tensile stresses. When the tensile capacity is exceeded cracks will develop. Additional deformation will follow until the steel strain is high enough that the additional steel force is equal to the released force by concrete cracking. On the compression side of the cross section these additional deformations cause a concentration of the concrete stress at the boundary of the cross section. Within the FE method the stresses close to the boundary of the elements are in general not related to the constitutive law since the stress recovery points are located within the element. (As long as the Gauss-Legendre quadrature is employed, which is standard in a FE analysis). A way to overcome this lack is to employ more sample points. When plates are analyzed it is common to employ more sample points over the depth (z-axis) of the plate compared to the number of sample points along the x- and y-axis of the plate. Within a 3D analysis stresses may have the steepest gradient in any direction, thus more sample points would be necessary for each direction in order to reproduce the technique employed in the 2D analysis. This is computational expensive, since the number of sample points increase by the power of three.
In Zienkiewicz [8] the influence of the integration order in situations of distorted elements is presented. A higher integration scheme is necessary in order to integrate the element stiffness more accurate. However, in the subsequent computation other errors occur. Some of these errors cancel out and satisfactory results can be achieved by employing a standard integration scheme (2x2x2 or 3x3x3). The example presented below concentrates on the physical nonlinearity of reinforced concrete. The effect of the stress recovery technique and the integration scheme for the residual forces on the results is studied and compared to analytical solutions.

5.1 Investigated Configuration

A single span beam as presented in Figure 11 is investigated. It is modeled with 48 elements. The elements are three dimensional and parabolic shape functions are employed. The beam is 600cm long, the cross section is 20/40cm. The system axis of the reinforcement has a distance of 5cm from the bottom end of the cross section. The concrete (f_c = 30.0MPa, f_t = 3.0MPa) is modeled with Ottosen failure criterion [20] according to Modelcode 90 [21]. The material is assumed to be linear elastic within the yield envelope (E_c = 30.000MPa). Mode I cracks are simulated by combining the Ottosen model with the Rankine tension cut off. The steel behavior is modeled linear elastic/perfectly plastic. (f_s = 550.0MPa, E_s = 200.000MPa). On both ends a moment is applied as load. For all cases studied in section 5.2 the magnitude of this moment is 0.016MNm. In section 5.3 the ultimate moment will be computed.

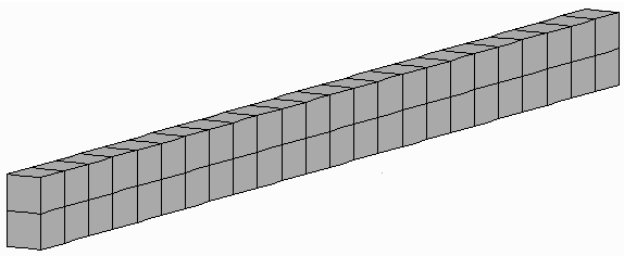

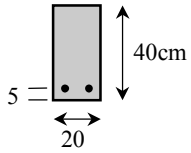

Concrete:
E_c = 30.000MPa
f_c = 30,0MPa
f_t = 3,0MPa

Steel:
E_s = 200.000MPa
f_s = 550,0MPa

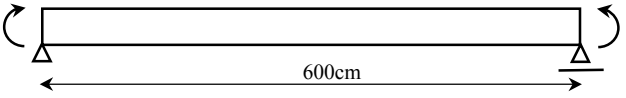

Figure 11 3D image, cross section and structural system of the investigated single span beam subjected to end moments

5.2 Beam subjected to service load

Figure 12 shows the stress distribution for plain (unreinforced) concrete before cracking. In this case the material behaves linear elastic. The numerical results with 2 sample points employed for the stress recovery coincide with the analytical solution as indicated in Figure 12.

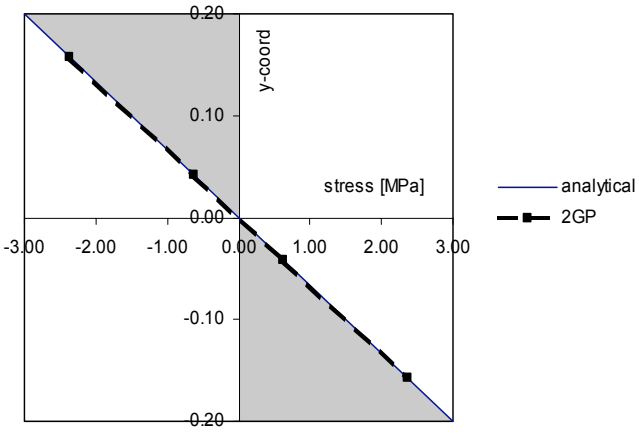

Figure 12 stress distribution of uncracked concrete, plain (unreinforced) situation, M = 0.016MNm

The distribution of stresses for the reinforced uncracked beam is shown in Figure 13. The beam is reinforced with 5 bars ϕ30mm, that is a very high reinforcement ratio. The numerical solution is identical to the analytical solution for the concrete stress and for the steel stress.

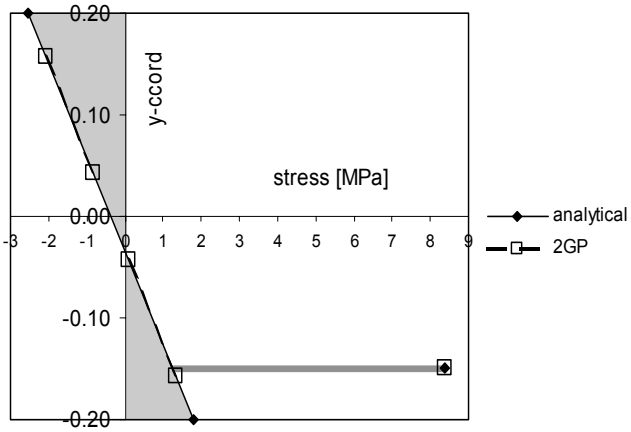

Figure 13 stress distribution of uncracked concrete, reinforcement: 5ϕ30mm, M = 0.016MNm

The distribution of stresses for the same configuration as discussed in Figure 13, but assuming cracked conditions for the concrete is shown in Figure 14. The constitutive relation for the concrete in compression is still linear. In this case, the analytical solution can be simulated very closely with 2 stress recovery points. However, a lower reinforcement ratio results into raising the neutral axis of the beam and an offset of the numerical solution will follow, since the integration will assume a wedge of tensile concrete stresses at the lower end of the upper element. These effects will be studied later on in Figure 15.

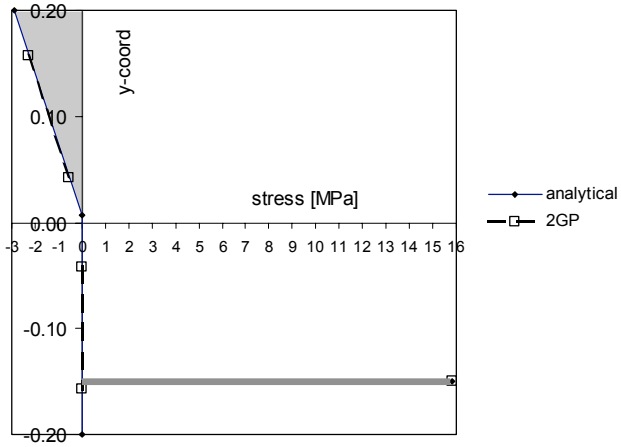

Figure 14 stress distribution of cracked concrete, reinforcement: 5ϕ30mm, M = 0.016MNm

For the example studied in Figure 15 the reinforcement is changed to 2ϕ12mm, that is approximately the minimum reinforcement required by design codes. The neutral axis of the beam rises. The stress distribution cannot be simulated well with two sample points in each direction. The concrete stress is underestimated and the steel stress is overestimated. However, equilibrium of external and internal forces is still fulfilled. Predicted strains are still in a close agreement to the analytical solution as shown in Figure 15b. Thus, more sample points are only required if a more accurate prediction of the concrete stresses is subject of interest. The analytical strains were computed based on the assumption of a linear elastic / no tension material.

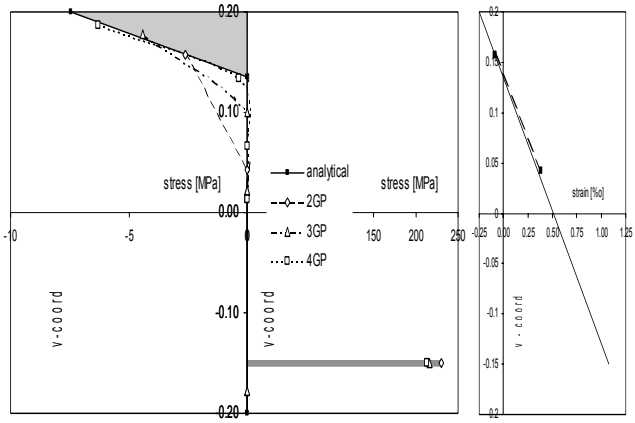

a) concrete stress / steel stress distribution b)strain distribution

Figure 15 stress distribution of cracked concrete, reinforcement: 2ϕ12mm, M = 0.016MNm

5.3 Beam subjected to failure load

The load is now monotonically raised for the low reinforced (2ϕ12mm) cross section. At a certain load level the steel stress reaches the yield limit. This load level is very close the ultimate load, since no further redistribution of tensile forces is possible. However, a small increase of the load is still possible since the neutral axis raises a bit due to the yielding of the steel. Thus, the cantilever of internal forces increases and the failure load does also increase therefore. The final distribution of concrete stresses is presented in Figure 16.

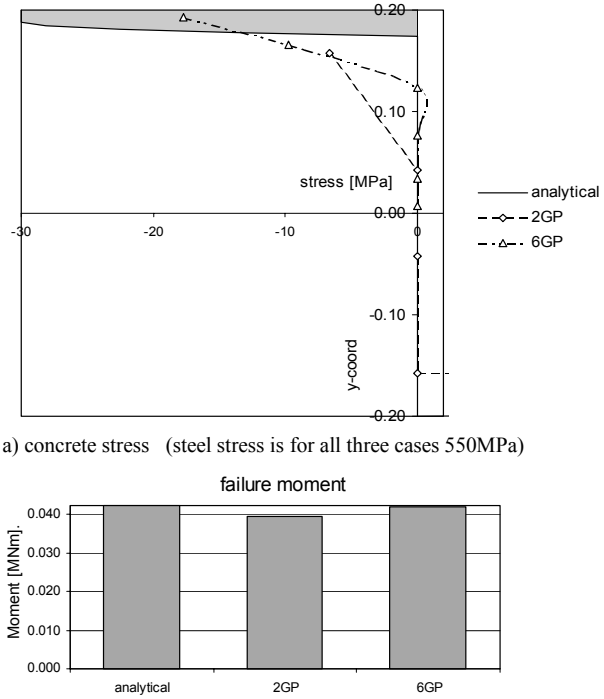

a) concrete stress (steel stress is for all three cases 550MPa)

Figure 16 failure load analysis; reinforcement: 2ϕ12mm (≈ minimum reinforcement)

The analytical solution shows a concentration of compression forces in the upper region of the cross section only. This stress concentration cannot be accounted for by employing two sample points in each direction, the concrete stresses are under predicted. The failure load is underestimated since the cantilever of the inner forces is shorter than the analytical one (the ultimate load is the yield force of the steel times this cantilever of the internal forces). However, although the concrete stresses are severely under predicted, the error of the failure moment is small in magnitude and on the save side. If 6x6x6 sample points are employed, the concrete stresses are predicted better but still poor in this specific case of low reinforcement ratio. The computational effort increases tremendously since 6x6x6 = 216 sample points have to be considered over the whole element instead of 8 for the 2x2x2 case. The ultimate moment can be computed close to the analytical solution. However, the failure moment computed with 2x2x2 sample points is not poor either.

In Figure 17 is the reinforcement increased to 2ϕ30mm. This is approximately the maximum reinforcement allowed by design codes for this beam. Beyond this limit, the beam would not be able to show a ductile failure, since failure would be initiated by a sudden crushing of the concrete and not by a ductile yielding of the steel. Due to the high reinforcement ratio, the capacity of the concrete is utilized highly. When 2x2x2 sample points are employed, the computed concrete stresses are satisfactory in the integration points, but the integration assumes a extrapolation of stresses. Thus, the stresses above the upper integration points will extrapolated beyond the limit stress. This is indicated by the gray shaded triangle in Figure 17. The concrete stresses are truly overestimated. However, the computed failure load is not overestimated. It is very close to the analytical one but still a bit lower. The error is on the save side again. The distribution of the concrete stresses computed with the 6x6x6 sample points is in good agreement with the analytical data. The concrete stress at the upper boundary of the cross section is negligible over predicted. The prediction of the ultimate moment is good as well, but the computational expense is high when six points are employed in each direction.

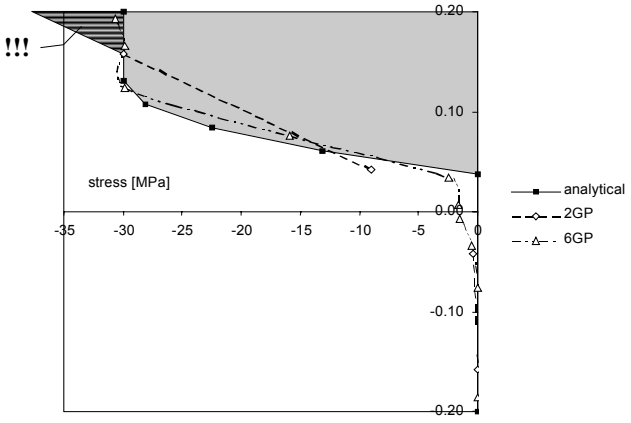

a) concrete stress (steel stress is for all three cases 550MPa)

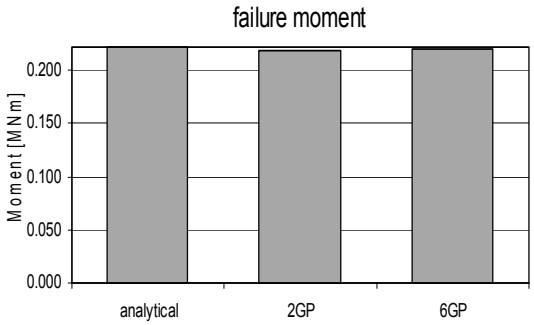

Figure 17 failure load analysis, reinforcement: 2ϕ30mm (≈ maximum reinforcement)

Following conclusions can be drawn from this example: A standard scheme (2x2x2 or 3x3x3 sample points) is able to compute the deformations well. Concrete stresses can be predicted well with the standard sample points only in such configurations where the stresses are not concentrated at the outer boundary of the element. This is of minor importance for computing the failure load since failure must be indicated by a yielding of the steel due to a design code requirement in order to obtain always a ductile failure mechanism. A accurate prediction of concrete stresses can be achieved in two ways. The first way is to refine the mesh in the regions of high concrete stresses. The second way is to employ more sample points for recovering the stress distribution. For computational reasons it is disregarded to employ too much sample points for every run. Thus it is recommended to use a mesh which is able to approximate the expected deformations in a satisfying way for the parameter studies. When the computation shows once promising results for a given set of parameters, a final run where computing time plays a minor role can be done with more sample points in order to compute more accurate concrete stresses as well.

6 REFERENCES

[1] Owen D. R. J., Hinton E., *"Finite Elements in Plasticity - Theory and Practice"*, 1980, Pineridge Press, Swansea

[2] Elwi, A.E., Hrudey, T.M., *"Finite Element Model for Curved Embedded Reinforcement"*, Journal of Engineering Mechanics, ASCE, , 1989, 115(4), pp. 740-754

[3] Beer, G., *"An isoparametric joint/interface element for finite element analysis"*, Int. J. f. Num. Meth. Engng., 1985, 21, pp. 585-600

[4] Hartl, H., Elgamal A., *"Nicht lineare kontinuumsmechanische Modellierung vorgespannter Konstruktionen (Non Linear Modeling of Prestressed Structures based on a Continuum Mechanics Approach)"* (in English), Heft 45 / September 2000, Österreichische Vereinigung für Beton- und Bautechnik, Vienna, pp. 87-96

[5] Hartl H., Sparowitz L, Elgamal A., "The 3D computational Modeling of Reinforced and Prestressed Concrete Structures", Bergmeister K. (ed.), Proceedings of the 3rd International PhD Symposium in Civil Engineering, Vienna, 2000, vol. 2, pp 69-79

[6] Crisfield, M. A., *"Non-linear finite element analysis of solids and structures"*, 1997, Wiley

[7] Nyssen, C., *"An efficient and accurate iterative method allowing large incremental steps to solve elasto-plastic problems"*, Computers&Structures, 1981, 13, pp. 63-71

[8] Zienkiewicz, O. C., Taylor, R. L., *"The finite element method"*, 4th ed, 1989, vol. 1, McGraw-Hill

[9] Beer, G., "BEFE user's and reference manual", CSS, Graz, 1999

[10] Hartl, H, "3D Computational Modeling of Reinforced Concrete Structures with Application to Soil Structure Interaction", Doct. Thesis, TU-Graz, in prep.

[11] Potts, D., Zdravković L., "Finite elements in geotechnical engineering", Thomas Telford, 1999

[12] Crisfield, M. A., *"Consistent schemes for plasticity computation with Newton-Raphson*

method", Computational Plasticity: Models, Software and Applications, Part 1, Pineridge, Swansea, 1987, pp. 133-259

[13] Oritz, M., Simo, J. C. *"An analysis of a new class of integration algorithms for elastoplastic constitutive relations"*, Int. J. f. Num. Meth. Engng., 1986, 23, pp. 353-366

[14] Perzyna P., *"Fundamental problems in viscoplasticity"*, Advances in Applied Mechanics, 1966, 9, pp. 243-377

[15] Perzyna, P., *"The Constitutive Equations for Rate Sensitive Plastic Materials"*, Quarterly of Applied Mathematics, 1963, 20(4), pp. 321-332

[16] Beer, G., Watson J.O., *"Introduction to Finite and Boundary Element Methods for Engineers"*, 1992, Wiley

[17] Cormeau, I., *"Numerical Stability in Quasi-Static Elasto/Visco-Plasticity"*, Int. J. f. Num. Meth. Engng., 1975, 9, pp. 109-127

[18] Zienkiewicz O. C., Cormeau I.C., *"Visco-Plasticity - Plasticity and Creep in Elastic Solids - A Unified Numerical Solution Approach"*, Int. Journal f. Num. Meth. in Engineering, 1974, 8, pp. 821-845

[19] Hartl, H., *"Implementation of Advanced Constutitive Model for Geomaterials into a Finite Element Code"*, Diploma-Thesis, TU-Graz, 1997

[20] Ottosen N.S., *"A Failure Criterion for Concrete"*, Journal of the Engineering Mechanics Division, ASCE, 1977, 103, pp. 527-535

[21] CEB-FIP Comitè Euro-International du Bèton, *"CEB-FIP Model Code 1990"*, 1993, Thomas Telford